# Kinematical views of mixing of fluids and granular materials: a brief review and open questions*

Julio M. Ottino
*Robert R. McCormick School and Engineering and Applied Science, Northwestern University*
*Evanston, Illinois 60208-3120, USA*

Recibido el 11 de noviembre de 1997; aceptado el 9 de febrero de 1998

## 1. Introduction

We outline examples of *fluid-fluid* mixing and *solid-solid* mixing highlighting kinematical issues. The fluid mixing case corresponds to the mixing of a fluid with itself; the flow is driven by boundary motions and 2D and 3D examples are considered. The solids case—mixing of granular matter—focuses on non-cohesive particles, possibly differing in density, mixed by rotation. Two subcases are considered: *slow flow*, where distinct avalanches occur, and *continuous flow*, where flow is restricted to a thin continuously avalanching layer, the rest of the granular material rotating as a single solid body. Open areas are identified throughout.

## 2. Mixing of fluids

Let us start by asserting that knowing where fluid particles are advected by a prescribed velocity field is the solution to a mixing problem. The solution of

$$\frac{d\mathbf{x}}{dt} = \mathbf{v}(\mathbf{x}, t)$$

with

$$\boldsymbol{\nabla} \cdot \mathbf{v} = 0, \tag{1}$$

where $\mathbf{v}(\mathbf{x}, t)$ is the Eulerian velocity field, gives the "flow" or "motion",

$$\mathbf{x} = \boldsymbol{\Phi}_t(\mathbf{x}_0),$$
$$\mathbf{x}_0 = \boldsymbol{\Phi}_{t=0}(\mathbf{x}_0), \tag{2}$$

that is, the particle with position $\mathbf{x}_0$ at time $t = 0$ is mapped to the position $\mathbf{x}$ after a time $t$ via a (nonlinear) flow $\boldsymbol{\Phi}_t(\cdot)$. The basic question is under what conditions is $\mathbf{v}(\mathbf{x}, t)$ able to produce mixing? A geometrical view helps. The classical view is that streamlines confine flows. This is certainly true in 2D systems but not true in unsteady, and particularly, time periodic flows 2D flows or steady 3D flows. A time periodic flow, $\mathbf{v}(\mathbf{x}, t) = \mathbf{v}(\mathbf{x}, t + T)$, can be represented by a map

$$\mathbf{x}_{n+1} = \mathbf{F}(\mathbf{x}_n)$$

or

$$\mathbf{x}_n = \mathbf{F}^n(\mathbf{x}_0), \tag{3}$$

where $n$ successive applications of the (nonlinear) point transformation $\mathbf{F}$ gives the position of the fluid particle initially located at $\mathbf{x}_0$ after $n$ periods of the flow. A periodic point, $\mathbf{p}$, of the (nonlinear) mapping, $\mathbf{F}$, is a point such that a particle initially located at $\mathbf{p}$ returns to $\mathbf{p}$ after $n$ periods, that is $\mathbf{p} = \mathbf{F}^n(\mathbf{p})$, where the periodicity $n$ is the smallest value satisfying the equality. Similar maps can be constructed by means of surfaces of section (Poincaré sections) in 3D flows. Let us restrict our discussion to 2D maps. Periodic points of 2D maps can be classified as hyperbolic, elliptic, or parabolic, according to the nature of deformation of the fluid in the neighborhood of the periodic point. A small circle surrounding an elliptic point returns to its original position and undergoes a net rotation. Elliptic points are surrounded by *islands*, or *regular regions*, where there is no chaos. Typically, the lowest period points are associated with the largest islands. In 3D systems islands represent the cross section of invariant tori.

These points are nicely illustrated by experiments [1]. Dye structures in time-periodic flows evolve in an iterative fashion: an entire structure is mapped into a new structure with persistent large-scale features, and with finer and finer scale features revealed at each period of the flow. Thin striations are produced at the expense of thicker ones, and length scales (characterized by a striation thickness) decrease exponentially in time. Islands translate, stretch, and contract periodically. Although islands undergo a net rotation, they preserve their identity, and represent the primary obstacle to efficient mixing. On the other hand, particle trajectories in chaotic regions separate exponentially fast, and material filaments are continuously stretched and folded by means of horseshoes. This area is reasonably well understood [2] (see Fig. 1).

As opposed to 2D case the number of theoretical studies addressing chaos and mixing in 3D flows is small [3] this can be attributed to the fact, that until now, there has not been an experimentally tractable bounded 3D system that allows for detailed computational investigation. Let us consider here a system inspired by the "chaotic droplet" model of Bajer and Moffat [4] and Stone *et al.* [5].

The apparatus consists of a cylindrical tank of diameter $T$ with a flat disk impeller with diameter $D$; the liquid level is denoted as $H$. Both the impeller and the tank can be rotated at angular speeds $\Omega_{\text{in}}$ and $\Omega_{\text{out}}$, respectively, and the angle of the impeller with respect to the vertical, $\alpha$, can be changed (see Fig. 2). The impeller's rotation creates a secondary flow,

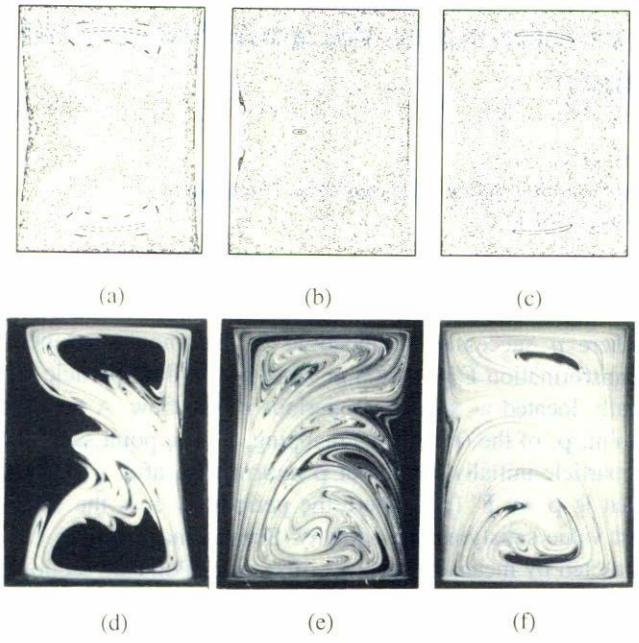


FIGURE 1. Chaotic mixing in time-periodic cavity flows. Experiments and computations reported in Ref. 2. The top and bottom walls move in counter-rotating directions. Top figures (a, b, c) are computed Poincaré sections, bottom figures (d, e, f), experiments with passive tracers. The displacement of the walls, the numbers of widths units the walls move in one period are (a) 4.62, (b) 6.93, and (c) 9.24.

towards the impeller and then radially outwards; at the same time rotation creates a twist. The combination generates nested nested tori above and below the impeller. Denote as $\alpha$ the angle between the impinging vortical flow and the axis of rotation. When the flow is axisymmetric ($\alpha = O$), the unstable manifold of the lower fixed point joins smoothly with the stable manifold of the upper fixed point, and both coincide with the axis of symmetry. In this case all the remaining trajectories lie on nested invariant tori. Perturbation of the geometry ($\alpha > 0$) results in chaos from two sources: the manifolds of the fixed points intersect resulting in homoclinic tangles near the axis, and some of the l-tori break into higher order tori surrounded by homoclinic tangles. In the Poincaré section the l-tori appear as closed curves and the higher order tori as a chain of islands. The tori with the most irrational winding numbers survive the greatest magnitude of perturbations.

KAM tori (islands of regularity in 2D cuts) are revealed clearly in 3D experiments. Higher period islands have not been experimentally captured in 2D experiments (islands in 2D experiments are, in general, only indirectly visualized; a blob placed in the chaotic region stretches to fill the entire chaotic region, the remaining area being the regular island; in fact, it normally takes thousands of periods to define the contour of an island in numerical Poincaré sections). The finite thickness of the experimental streaklines, which results in the streaklines being stretched into sheets or ribbons, facilitates visualization. Islands in the Poincaré section result from the

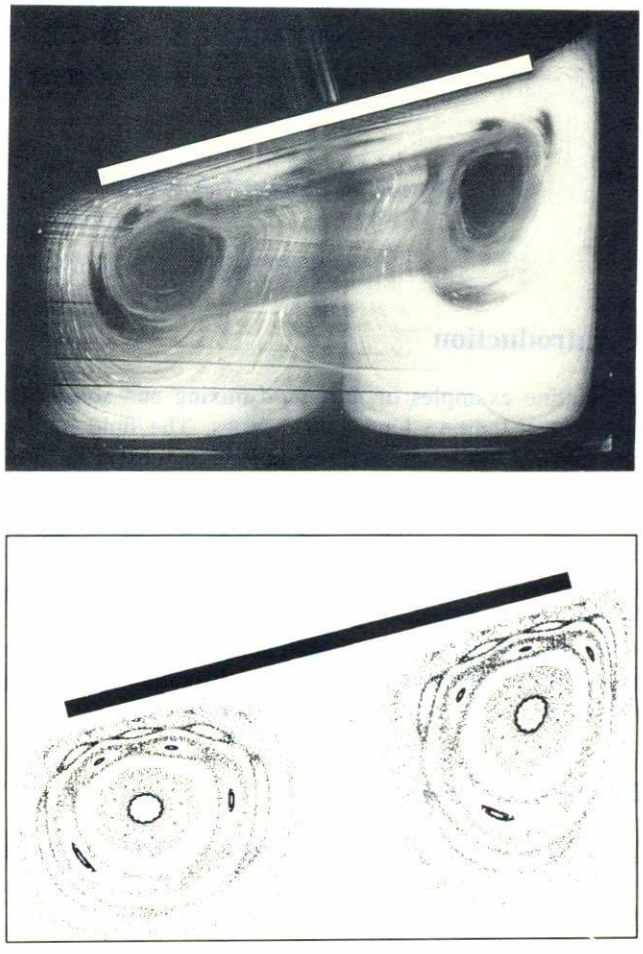

FIGURE 2. Chaotic 3D advection in the "fundamental mixing tank". Top figure, experiment; bottom figure, Poincaré section. The Reynolds number of the flow is about 7.0 (G. Fountain *et al.*, in progress).

the intersection of tori with the laser-illuminated surface. The robustness of these analog (experimental) simulations lies in their ability to produce connected structures, *versus* the "peppered-like" appearance of computational results involving tracking of single particles. There is a need for experimental and theoretical studies of mixing in 3D flows.

What happens if the fluids are changed? There are no experiments we know of addressing this issue in 3D and only a handful in 2D. Niederkorn and Ottino [6] studied experimentally and computational mixing of Boger fluids—a viscoelastic fluid with a constant shear viscosity—in the 2D flow between two concentric cylinders. In the limit of slow flow, a Boger fluid behaves as Newtonian; faster flows lead to viscoelastic effects quantified in terms of Weissenberg number ($We$), the ratio of the relaxation time of the fluid to a time scale of the flow; *e.g.* the inverse of the shear rate. Spectacular effects occur at moderate $We$; Figure 3 shows the contrast between the Newtonian ($We \cong 0$) and the non-Newtonian case ($We = 0.06$). We know of only one paper addressing the explanation of these effects [7].

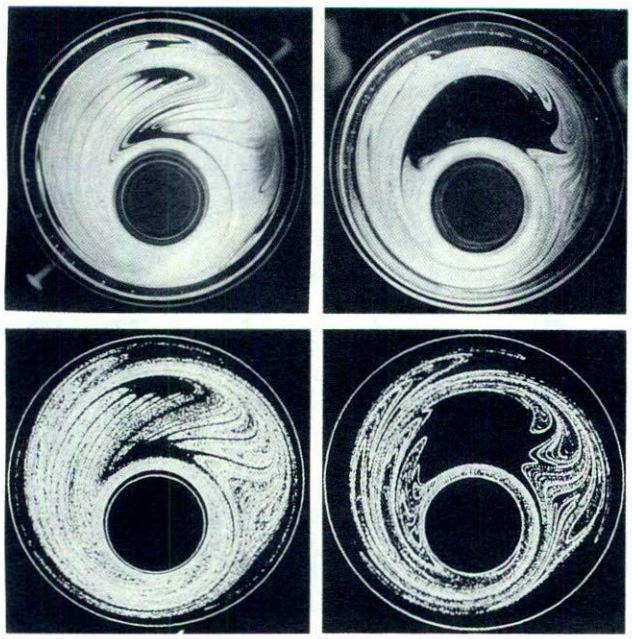

FIGURE 3. Chaotic advection of viscoelastic (Boger) fluid in a time period flow. The top row corresponds to experiments, the bottom row to computations. The left column corresponds to the Newtonian limit ($We \cong 0$); the right column to $We \cong 0.06$.

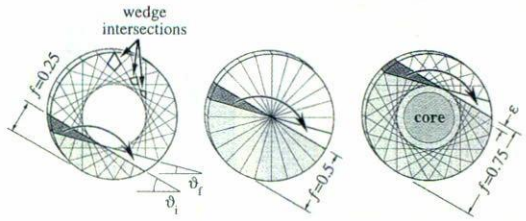


FIGURE 4. Avalanches for various degrees of filling, denoted $f$. The figure for $f = 0.25$ shows that a wedge, after avalanching and undergoing solid body rotation, becomes part of a new avalanching wedge. This is the primary mixing mechanism. At $f = 0.5$ the wedges have no intersections and the mixing vanishes; for $f = 0.5 + \varepsilon$, where $\varepsilon$ is a boundary layer thickness, a core forms. The last frame shows the core for $f = 0.75$.

## 3. Mixing of solids

A general initial caveat is necessary: In mixing of solids *mixing* and *unmixing* (segregation) come together. Granular mixtures of dissimilar (and not-too-dissimilar) materials often segregate when shaken or tumbled. Thus, for example, differences in size result in *percolation* of smaller particles in flowing layer [8], differences in *size* [9] or *density* [10] result in *radial* segregation (formation of a segregated core of smaller or more dense particles) in the flow in rotating cylinders, and differences in the *angle of repose* result in the formation of *axial bands* in the flow in rotating cylinders [11, 12]. Radial segregation becomes evident after 5–10 revolutions, axial segregation taking at least an order of magnitude longer.

Consider first the case of flows of identical particles. Granular flow in a horizontal rotating cylinder and can be classified into different regimes [13], at low rotational speeds the flow consists of discrete avalanches: one stops before the next one begins (the *avalanching* or *slumping* regime). At higher speeds a steady now is obtained with a thin cascading layer at the free surface of the rotating bed (*contiuous flow, rolling* or *cascading* regime; see Fig. 3a). At still higher speeds particle inertial effects become important and particles may become airborne (*cataracting* regime). Evidence for radial segregation has been presented in a number of previous works [14–16] it has however, been the primary subject of study of only a few recent papers [17, 18].

Consider mixing by tumbling in the prototypical tumbling system: a rotating 2D drum partially filled with identical (except for color) granular particles. If the rotation speed is sufficiently slow the angle of the free surface ($\theta$) grows until a discrete avalanche occurs, and $\theta$ relaxes from its pre-avalanche angle, $\theta_i$, to a new angle, $\theta_f$. These two angles define two wedges, the before and after positions. As the avalanche occurs, material in the uphill wedge flows to fill the downhill wedge.

There are two types of maps in this case: a coarse map defining the gross motion of material during an avalanche—a wedge goes into a new wedge—and a finer map describing the detailed motion within the wedge. Thus the motion can be decomposed into two components: a geometrical component, consisting only of the transport of the wedges, and a dynamical component, consisting of a complex rearrangement of material within the wedge as a result of this transport.

However well or poorly dynamical mixing occurs within a wedge, material cannot be transported outside of the wedges during an avalanche. Thus global mixing from material in one wedge into a different wedge can only occur within quadrilateral intersections between wedges. Second, at a fill level of 50%, the quadrilateral intersections vanish. Consequently we expect global mixing to vanish for a half-filled drum. Third, the quadrilaterals expand as the fill level diminishes, so we expect global mixing to improve for lower fill levels. Fourth, fill levels greater than 50% produce a core in the center of the granular mass. No wedges penetrate the core, so no mixing should occur there. All of these predictions are validated by experiments [19].

Quantitative predictions require a description of the mixing within the wedge. The simplest assumption is that particles are completely randomized following each avalanche (this is accomplished by interchanging every particle within the final wedge with another particle, also within the final wedge, chosen at random). This is what was done to generate the simulations shown at the bottom of Fig. 5a. Figure 5b shows mixing rates calculated for this problem. As predicted, the mixing rate goes to zero for half full drums, and increases as the fill level is reduced. Some mixing occurs for fill levels

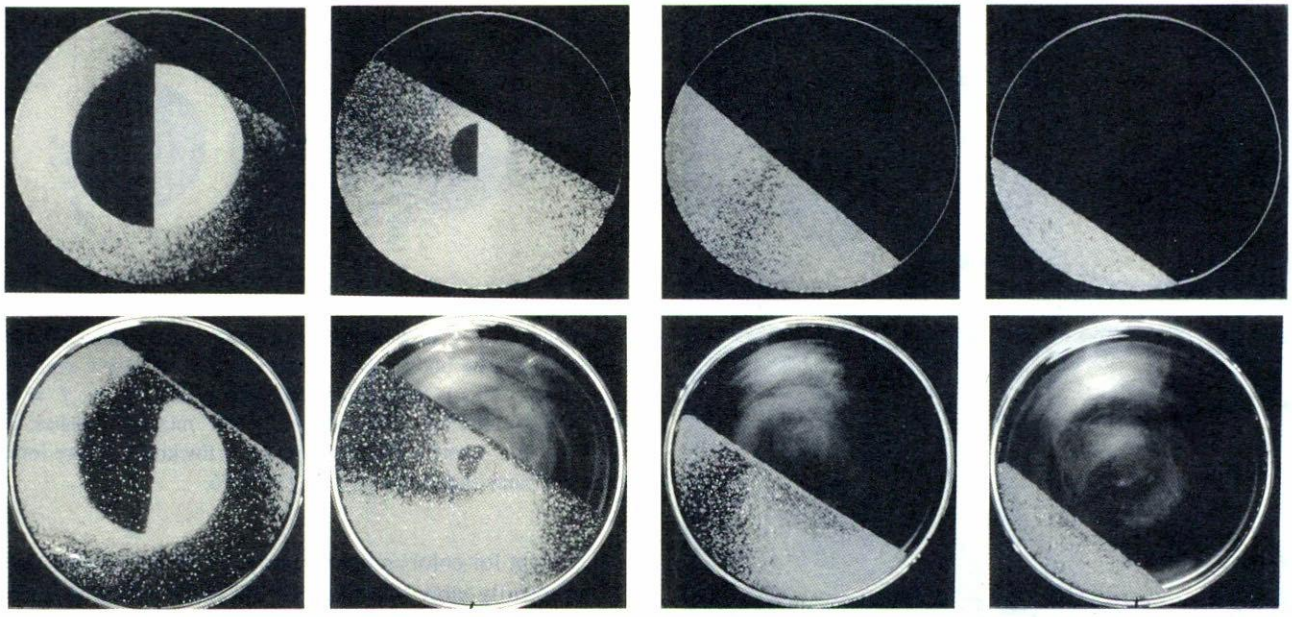

FIGURE 5a. Predictions of avalanche model. Top row shows the model predictions the bottom row, experimental results. The fill levels, $f$, from left to right are 0.8, 0.6, 0.4, and 0.2. The material was initially segregated with a vertical interface dividing two equal parts, as can be seen in the largest unmixed core in the left column.

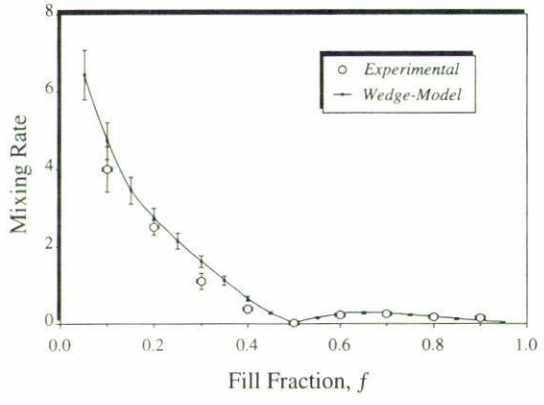


FIGURE 5b. The graph shows a quantitative prediction of the mixing rate as function of the fill level and a comparison with the experimental results (the "mixing rate" is the constant in the exponential decay, measured as the approach between the approach of the center of masses of the two materials).

els over 50%, although the mixing is substantially impeded by the core (even taking into account the fact that the mixing rate in the figure excludes the core).

The geometric viewpoint survives even if particles are changed, provided that they are not so cohesive that distinct angles of repose become ill defined. In this respect, the geometric view is more robust for solids than for fluids, where a change in rheology can have drastic effects on the structure of the resulting flow (*cf.* Fig. 3).

In both examples, mixing of fluids and mixing of solids, there are features that do not mix. In fluids, these are islands or tori, in solids, these are cores. In both problems, outside of these regions, mixing can be good, and an understanding of the causes of these impediments to mixing can be used to avoid them. To see this in the solids case, we note that the cause of the core is that mixing avalanches do not penetrate into this region. By including baffles, we can deliberately cause avalanches to penetrate the core, and thereby involve it in mixing. The mechanism at work is subtle. In Fig. 6, we show a sequence of sketches depicting what occurs as a tumbler with protruding baffles is slowly rotated. Initially, avalanches penetrate part way into the baffle, but the granular flow is eventually impeded by the upper corner of the baffle. Because granular flows can support a load, the cavity within the baffle remains for some period as the drum continues to rotate. After a certain point, however, the angle made by the baffle becomes sufficiently steep that the grains near the cavity collapse, and the supported material likewise settles. As this happens, the core shifts downward, and this shifting permits material on the outer edges of the core to enter the mixing zone. In this way, the core can be steadily eroded.

This brings us to a second similarity between fluids and solids, namely that symmetries interfere with mixing in both problems. As an example of this we may mention the case of two different baffle designs. It might be thought that two baffles would accomplish twice the erosion of the core shown in Fig. 6. In fact the symmetric placement of baffles results in the core shifting in one direction during one half of the rotation cycle and in the opposite direction during the second half cycle. Consequently the core undergoes no net translation, and steady erosion does not occur.

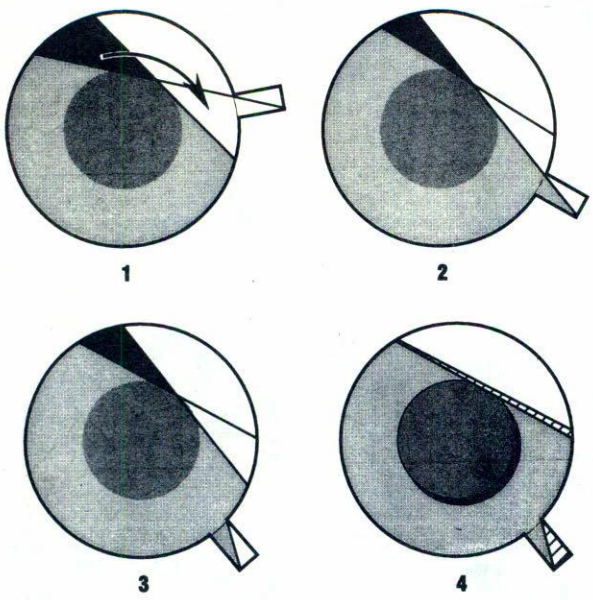


FIGURE 6. Mixing by avalanches in circle with a protruding cavity. As the material yields and invades the cavity the core is displaced and eroded.

Another example is the case of 3D cylinders, where one may want to enhance axial mixing as well as radial mixing. In the slow rotation regime, radial mixing (possibly excepting the core for mixers filled beyond 50%) may be accomplished by avalanching. Under such conditions the axial mixing is very slow since it is essentially diffusive. Substantially faster overall mixing can be achieved by a combination of rotation and "wobbling" of the axis of the cylinder. Wobbling creates avalanches along the axial direction [20], the interplay between avalanches enhances the mixing.

Other lessons from fluid analysis carry over to the solids case as well. Steady flows in fluids are poor mixers. For the solids case, a similar message holds. Consider the drum mixer spun at a faster rate than before, so that the surface layer flows continuously; one can break the problem in two: a bulk region, which rotates as a solid body with the drum, and a surface layer, where mixing can occur. Here the flow is steady, and we expect that *at equal number of rotations*, that the mixing will be less than in the time-periodic avalanching regime.

Consider first a few details of the continuous flow in a cylinder of radius $L$ rotating at speed $\omega$. In the continuous flow regime the surface flow of direction $x$ and normal $y$ is confined to a thin layer of lenticular-like shape along a free surface along $-L < x < L$ which is nearly flat. The overall flow is comprised of two parts: nearly unidirectional flow in the cascading layer and solid body rotation in the bed. For fill levels close to 50%, the volume flux in the layer, assuming the total particle volume friction ($\phi_t$) to be nearly the same in the fixed bed and the cascading layer, is given by

$$\langle v_x \rangle \delta = \frac{\omega L^2}{2}\left(1 - \frac{x^2}{L^2}\right) = Q, \tag{4}$$

where $v_x$ is the velocity along the layer, $\delta(x)$ is the layer thickness, and $Q = Q(x)$ is the volume flux per unit width in the layer at position $x$. The pointed brackets denote an average across the layer. This result is obtained solely on kinematical grounds and assumes only that the region of flow is thin. The velocity field can be obtained by assuming a nearly unidirectional flow [21]. Rescaling all distances with $L$, so that $\xi = x/L$, $\eta = y/L$ and time with $1/\omega$, implies that velocities are scaled with $\omega L$, and the flow rate with $\omega L^2$. The velocity field, flow rate, and the thickness of the layer are

$$\langle \bar{v}_x \rangle \bar{\delta} = \frac{1}{2}\left(1 - \xi^2\right) = \bar{Q}, \tag{5}$$

$$\bar{v}_x = 2\bar{u}\left(1 + \frac{\eta}{\bar{\delta}}\right), \quad \bar{v}_y = \xi\left(\frac{\eta}{\bar{\delta}}\right)^2, \quad \bar{\delta} = \bar{\delta}_0\left(1 - \xi^2\right), \tag{6}$$

where the overbar denotes dimensionless quantities; $\bar{Q} = Q/(\omega L^2)$ and $\delta_0 = 1/(2\bar{u})$. The only parameter of the flow is the maximum flowing layer thickness, $\bar{\delta}_0$, which can be directly measured.

Thus, a general model describing simultaneous mixing and segregation can be written as

$$\frac{\partial \phi_1}{\partial t} + v_x \frac{\partial \phi_1}{\partial x} + v_y \frac{\partial \phi_1}{\partial y} = \frac{\partial}{\partial x}\left(D\phi_t \frac{\partial f}{\partial x} - J_{sx}\right) + \frac{\partial f}{\partial y}\left(D\phi_t \frac{\partial f}{\partial y} - J_{sy}\right), \tag{7}$$

where $\mathbf{J}_s = (J_{sx}, J_{sy})$ is the segregation flux of the more dense particles, denoted $\phi_1$.

The driving force for segregation can be described in terms of an effective "buoyancy." Denote by $J_{sy}$ the segregation flux of the more dense particles and $\theta$ the angle of the surface flow with the $x$-axis. The segregation flux is

$$J_{sz} = -C\phi_1\left(\rho_1 - \langle \rho \rangle\right) g \cos\theta \tag{8}$$

where the average density is given by

$$\langle \rho \rangle = \frac{\rho_1 \phi_1 + \rho_2 \phi_2}{\phi_1 + \phi_2} \tag{9}$$

and $C$ is an unknown function which is a measure of the resistance to local motion this model has to be tested by particle dynamics and Monte Carlo simulations; all indications are that this model works reasonably well [22]. A challenge is to develop a companion model for the case of particle size segregation.

A Lagrangian approach can be used to obtain the dynamic evolution of the concentration distribution; particles are initially distributed randomly in the bed and advected by the flow, taking into account the segregation and diffusion fluxes.

Consider one example of the application of the theory's ability to reproduce experimental results. The objective is to homogenize an initially segregated mixture. In this case the dynamics of mixing and segregation interacl to give a complex evolution of the mixed state. Figure 7 shows an example of such a process, in which an

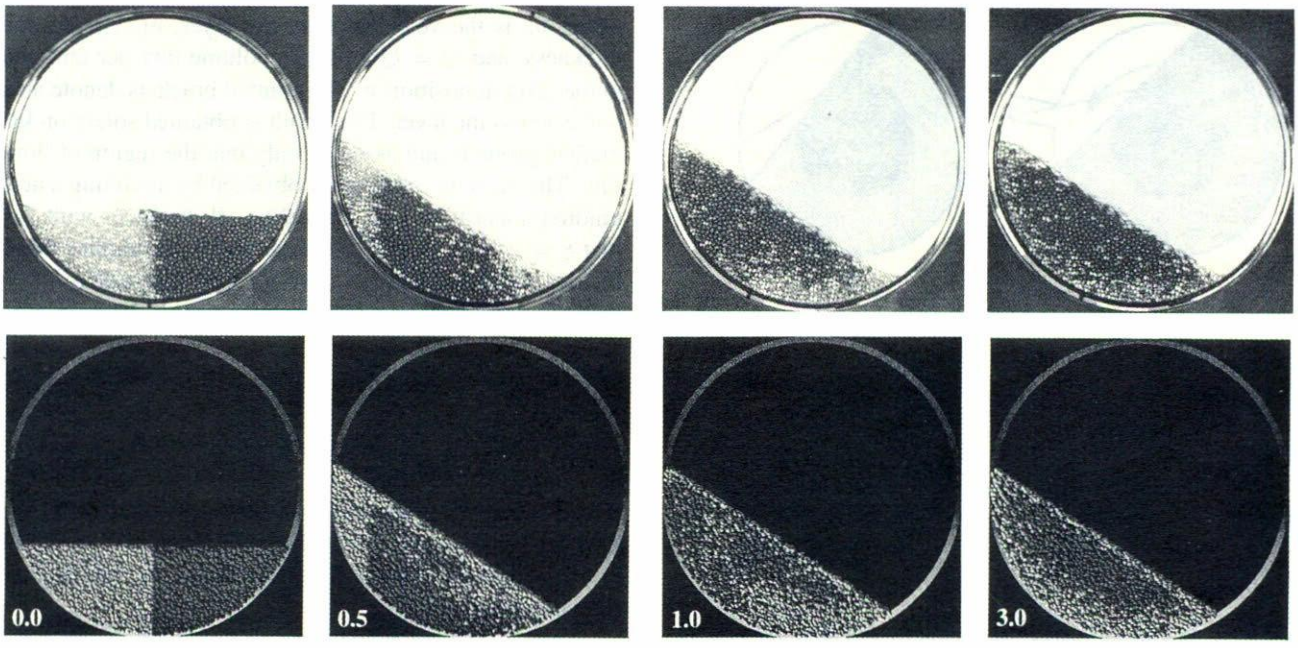


FIGURE 7a. Mixing and segregation in the continuous flow regime. The top row shows the experimental results; the materials are glass beads and steel balls of nearly equal sizes but differing in density by about 3.8. The numbers in the bottom row, computational results, indicate the number of revolutions. After three revolutions the denser material has migrated towards the center and the mixing becomes worse that after just one revolution.

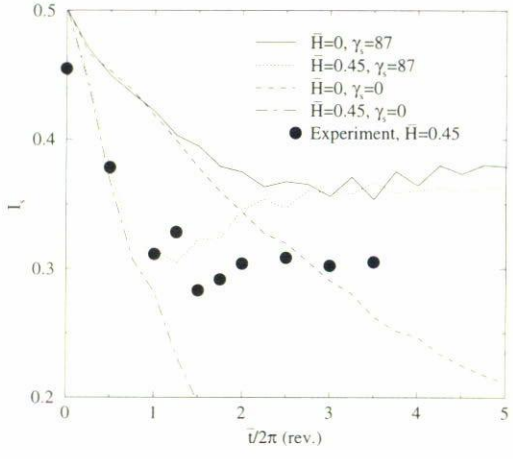


FIGURE 7b. The graph shows the evolution of the intensity of segregation, $I_s$, for different fill conditions and *net segregation fluxes*, $\gamma_s$. It is apparent that, depending on parameter values, the intensity of segregation, may go through a minimum before reaching steady state.

initially segregated state evolves to an equilibrium distribution (the continuum particles have been made the "same size" as the experiments to facilitate comparison). The agreement is quite satisfactory. Time evolution computations show that the model captures interesting trends: often the system is better mixed at intermediate times; after partial mixing the system unmixes. This becomes clearer if the mixed state at any time is quantified in terms of the *intensity of segregation* defined as

$$I_s = \left[ \frac{\sum_{i=1}^{N} (f_{bi} - f_T)^2}{N-1} \right]^{\frac{1}{2}} \tag{10}$$

where $\{f_{bi}\}$ are the number fractions at a set of $N$ points uniformly distributed in the bed, calculated from the particles in a square box of a specified size centered on each point and $f_T$ is the average for the entire bed. Figure 7b shows experimental and computational results for various degrees of filling and, in the case of computations, different *net segregation fluxes* ($\gamma_s$). Extensions of the theory and companion experiments need to be developed to investigate optimal mixing conditions in systems of practical interest.

A final comment, outlining a potentially fruitful area, may be in order. We stated earlier that steady flows are poor mixers. The flow in the cylinder in the continuous flow regime is steady, whereas the avalanching flow is time periodic. We therefore expect that *at equal number of rotations*, that the mixing in the time-periodic avalanching regime will be more effective. One may wonder however, if there are ways to improve the mixing in the continuous flow regime. The answer to this question is yes, but the potential implications remain to be explored. One possibility is to run the flow in an ellipse. Figure 8 shows two cases, for different degrees of filling, in term of Poincaré sections. It is apparent that they flow of granular materials can be chaotic.

FIGURE 8. Chaotic advection in ellipses of aspect ratio 0.7 in the contnuous flow regime. Different fill levels are shown. The right figure displays an unmixed central core (J. Glichrist, in progress)

## Acknowledgments

The work described here has been supported by the National Science Foundation, DOE, Division of Basic Energy Sciences, and The Petroleum Research Fund, administered by the American Chemical Society. This brief summary represents work carried out by Gerald Fountain, James Gilchrist, Devang Khakhar, Joseph McCarthy, and Troy Shinbrot. The papers quoted should be consulted for details that go beyond the brief descriptions outlined here.

---

*. Outline of plenary lecture delivered at the XL National Congress of Physics; Monterrey, Nuevo León, Mexico, October 1997.

1. J.M. Ottino, C.W. Leong, H. Rising, and P.D. Swanson, *Nature* **333** (1988) 419.
2. S.C. Jana, G. Metcalfe, and J.M. Ottino, *J. Fluid Mech.* **56** (1994) 199.
3. R.S. MacKay, *J. Nonlinear Sci.* **4** (1994) 329.
4. K. Bajer, H.K. Moffatt, *J. Fluid Mech.* **212** (1990) 337.
5. H.A. Stone, A. Nadim, and S.H. Strogatz, *J. Fluid Mech.* **232** (1991) 629.
6. T.C. Niederkom and J.M. Ottino, *J. Fluid Mech.* **256** (1993) 243.
7. S. Kuma and G.M. Homsy, *Phys. Fluids* **8** (1996) 1774.
8. S.B. Savage and C.K.K. Lun, *J. Fluid Mech.* **189** (1988) 311.
9. M.B. Donald and B. Roseman, *Br. Chem. Eng.* **7** (1962) 749.
10. G.H. Ristow, *Europhys. Lett.* **28** (1994) 97.
11. S. Das Gupta, D.V. Khakhar, and S.K. Bathia, *Chem. Eng. Sci.* **46** (1991) 1513.
12. K.M. Hill and J. Kakalios, *Phys. Rev. E* **52** (1995) 4393.
13. H. Henein, J.K. Brimacombe, and A.P. Watkinson, *Metall. Trans. B* **14B** (1983) 191.
14. S.S. Wiedenbaum, "Mixing of Solids", in *Advances in Chemical Engineering*, Vol. 2, edited by T.B. Drew and J.W. Hoopes, (Academic Press, N.Y., 1958), p. 211.
15. G. Metcalfe and M. Shattuck, *12th Australian Fluid Mechanics Conference*, Sydney, Australia, December 10–15 (1995).
16. K.M. Hill, J. Kakalios, and A. Caprihan, *World Congress of Chemical Engineering* (1996).
17. H. Hencin, J.K. Brimacombe, and A.P. Watkinson, *Metall. Trans. B* **16B** (1985) 763.
18. N. Nityanand, B. Manley, and H. Henein, *Metall. Trans. B* **17B** (1983) 247.
19. G. Metcalfe, T. Shinbrot, J. McCarthy, and J.M. Ottino, *Nature* **374** (1995) 39.
20. C. Wighttman, P.R. Mort, F.J. Muzzio, Re. Riman, and E.R. Gleason, *Powder Tech.* **84** (1995) 231; J.J. Mcarthy, T. Shinbrot, G. Metcalfe, J.E. Wolf, and J.M. Ottino, *AIChE J* **42** (1996) 3351.
21. D.V. Khakhar, J.J. McCarthy, T. Shinbrot, and J.M. Ottino, *Phys. Fluids* **9** (1997) 31.
22. D.V. Khakhar, J.J. McCarthy, and J.M. Ottino, *Phys. Fluids* **9** (1997) 3600.